Effect of Diamine Bridge on Reactivity of Tetradentate ONNO Nickel(II) Complexes

Kamila Pruszkowska,[*a] Olga A. Stasyuk,[*a,b] Anna Zep,[a] Adam Krówczyński,[a] Rafal R. Sicinski,[a] Miquel Solà[b] and Michał K. Cyrański [a]

[a] Faculty of Chemistry, University of Warsaw, Pasteura 1, 02-093 Warsaw, Poland

[b] Institut de Química Computacional and Departament de Química, Universitat de Girona, C/ Maria Aurèlia Capmany 69, 17003 Girona, Catalonia, Spain

*Corresponding authors

E-mail address: K.P. kpruszkowska@chem.uw.edu.pl; O.A.S. o.a.stasuk@gmail.com

ABSTRACT

Two new square planar ONNO nickel(II) complexes **C2_core** and **C3_core** have been synthesized and characterized by single crystal X-ray diffraction, NMR spectroscopy, thermogravimetry, and DFT calculations. The experimental results revealed the effect of the length of diamine bridge in the ligand on the behavior of the studied complexes in the reaction with *N*-heterocyclic aromatic amines, while DFT calculations provided a basis for the rationalization of this observation. The complex with propylenediamine bridge (**C3_core**) readily reacts with pyridine and its derivatives with the formation of high-spin (paramagnetic) complexes with octahedral geometry characterized by X-ray diffraction; electron-donating substituents on the pyridine ring facilitate the coordination of axial ligands. On the contrary, the complex with ethylenediamine bridge (**C2_core)** does not undergo such a reaction because of the high deformation energy of the core required for the formation of **C2_Py** complex.

INTRODUCTION

Nickel(II) complexes (d^8-configuration) can exist in singlet or triplet spin state. Square planar Ni(II) complexes are diamagnetic, with a singlet ground state (S = 0). However, when their geometry changes to square pyramidal or octahedral (with coordination number of five and six, respectively), these complexes become paramagnetic, with a triplet ground state (S = 1). Such transition between two spin states was denoted Coordination-Induced Spin-State Switching (CISSS). This effect was first discovered for Ni(II) by Herges and co-workers,[1-3] and later was observed for other transition metal complexes, e.g., Fe(II), Fe(III), Mn(II), Mn(III), and Co(II). Spin-state switching phenomena in transition metal complexes is currently an intensively studied area in coordination chemistry, because such systems have a potential for application in memory devices, chemical sensors, and contrast agents for magnetic resonance imaging.[4-8]

A number of Ni(II) complexes, in which the metal center is located in ONNO environment, have been synthesized previously.[9-13] The most common representatives of tetradentate ONNO ligands are found in the salen series, [salen = N,N'-bis(salicylidene)ethylenediamine].[13,14] However, their acacen analogues [acacen = N,N'-bis(acetylacetone)ethylenediamine] are much less frequently used as ligands in coordination chemistry and the library of their complexes with transition metals is significantly smaller.[9,15,16] The principal examples of such compounds are $[Co(acacen)L_2]^+$ complexes, which have been studied extensively as potential protein inhibitors (e.g., for selective inhibition of Human α-Thrombin).[17,18] Another prominent representative of such complexes is Fe(II) spin-crossover complex with the wide thermal hysteresis loop.[19,20]

Square planar nickel(II) complexes can change their coordination sphere by addition of donor ligands, this transformation can be detected by shifts in the UV–vis spectra.[1,3,13] Propensity of Ni(II) complexes towards formation of octahedral complexes depends on the nature of equatorial ligands and basicity of the axial ligand. The first structurally characterized octahedral nickel(II) complexes with acacen equatorial ligand were reported in 2010.[11] Recrystallization of Ni{N,N-ethylenebis(1,1,1-trifluoroacetylacetoneiminato)} [NiL] from pyridine resulted in brown crystals of $[NiL(Py)_2]$ characterized by X-ray diffraction. Moreover, the reaction with the bidentate ligand 1,4-diazabicyclo[2.2.2]octane (dabco) led to the formation of one-dimensional coordination polymer, in which dabco axially bridges [NiL] units in a linear fashion. It was noted that no corresponding solid products were formed in the absence of CF_3 groups in the equatorial ligand.[11] Thus, the incorporation of highly polar functional group (such as CF_3) near coordination sphere of transition metal plays the important role in the formation of octahedral complexes with N-donor ligands. Very recently, a family of planar nickel(II) complexes with four phenazine-based acacen-type ligands has been reported.[9] The complexes demonstrate CISSS behavior with fluorescence detection and can find application as molecular sensors. The addition of pyridine to them in the excited state is more favorable than in the ground state. The electron-withdrawing CF_3 substituents in the ligand strongly affect the acidity of the nickel center and facilitate coordination of axial ligands, increasing the CISSS sensitivity.

Here we report the synthesis and characterization of two new nickel(II) complexes based on acacen framework (Figure 1). We focused on such type of Ni(II) complexes because the acacen/acacpn ligands shown in Figure 1 are promising ligand platform, where phenyl rings can be easily functionalized with various substituents to tune the electronic properties of the resulting complex. The acacen type of ligands is based on N,N'-bis(acetylacetone)ethylenediamine, while acacpn ligands - on N,N'-bis(acetylacetone)propylenediamine. Studying the reactivity of these complexes towards pyridines, we found that only one of them is capable of forming octahedral complexes and changing its spin state upon coordination of axial ligands. In contrast to the above-mentioned research,[9,11] where electronic effect of substituents[21] plays the crucial role in the formation of octahedral Ni(II) complex, the results presented in this paper are strongly connected with geometric effect.

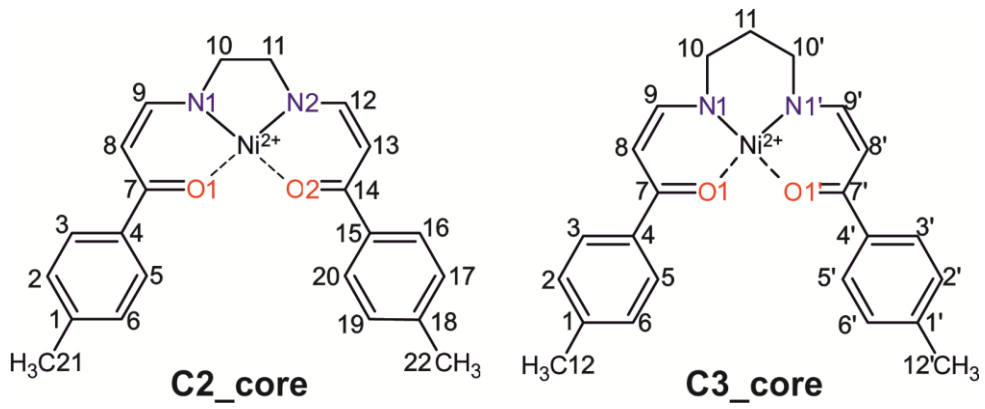

Figure 1. Molecular structure of studied Ni(II) complexes.

EXPERIMENTAL SECTION

X-ray crystallographic analysis

Single crystal X-ray diffraction data for **C2_core, C3_core**, **C3_Py**, **C3_DMAP** and **C3_MOPy** compounds were collected on D8 Venture single crystal diffractometer using MoKα radiation. The data treatment and reduction were done using the Bruker software suite.[22-25] Structures were solved and refined using SHELXT[26] and SHELXL[27] software with the atomic scattering factors taken from the International Tables.[28] The **C3_DMAP** structure was solved with the SHELXS[29] software using Direct Methods and refined with the olex2.refine[30] refinement package employing the Gauss-Newton minimization in Olex software.[31] The crystals of **C2_core** were twinned, which was taken into account in data reduction and structure refinement. A detailed description of data collection and structures refinement are presented in Supporting Information. Mercury CSD 4.1.0 software was used for the preparations of crystal structure figures.[32] Crystallographic data for the crystal structures described in this publication have been deposited with the Cambridge Crystallographic Data Centre with 2106933 – 2106937 deposition numbers.

Hirshfeld surface analysis

The Hirshfeld surfaces and two-dimensional fingerprint plots were generated using Crystal Explorer 17.5 to provide the information about intermolecular interactions in the crystal structures of **C2_core**, **C3_core, C3_Py** and **C3_MOPy**.[33-35] Due to significant disorder in the crystal structure in the case of **C3_DMAP**, the Hirshfeld surface analysis has not been made.

Theoretical methods

Geometry optimization of square planar Ni(II) complexes (**C2_core** and **C3_core)** and octahedral Ni(II) complexes (**C3_Py**, **C3_MOPy** and **C3_DMAP**) was performed in different spin states using ADF package.[36,37] BP86 functional[38,39] was used with TDZP basis set, which consists of triple-ζ quality basis set on the Ni and double-ζ quality on the other atoms, including one polarization function. Scalar relativistic correction ZORA,[40] D3 dispersion correction by Grimme,[41] and COSMO solvation model (pyridine with ε=12.4)[42] were included. To ensure that the obtained geometries are in energy minima, the vibrational analysis was performed and no imaginary frequencies were found. Single-point energy calculations with BP86 and S12g[43] functionals and TZ2P basis set were subsequently performed. The S12g functional is especially well-suited for studies of CISSS.[43,44]

Nuclear magnetic resonance

The ^{1}H NMR and ^{13}C NMR spectra were recorded on the Agilent (400 MHz) spectrometer. Proton chemical shifts were reported in ppm (δ) relative to the internal standard – tetramethylsilane (TMS: δ 0.00 ppm). Carbon chemical shifts were reported in ppm (δ) relative to the signal corresponding to the residual non-deuterated solvent ($CDCl_3$: δ 77.0). Data are presented as follows: chemical shift, integration, multiplicity (s = singlet, d = doublet, t = triplet, dd = doublet of doublets, br = broad, m = multiplet), and coupling constant (Hz), see Supporting information (SI).

Ultraviolet–visible spectroscopy (UV-Vis)

The UV-Vis absorption spectra were obtained on Shimadzu UV- 2401PC UV spectrophotometer in chloroform and pyridine.

Thermogravimetric analysis

Thermogravimetric analysis (TGA) was carried out with the TA Instruments Q50 Thermal Gravimetric Analyzer. The sample was measured in 20-700° range with 10K/min heating rate and the nitrogen as a purge gas.

RESULTS AND DISCUSSION

Square planar Ni(II) complexes

Ni(II) complexes with tetradentate ligand containing two (**C2_core**) and three (**C3_core**) carbon atoms in the bridge were synthesized according to the general procedure shown in Scheme 1. Details for each step of synthesis can be found in SI.

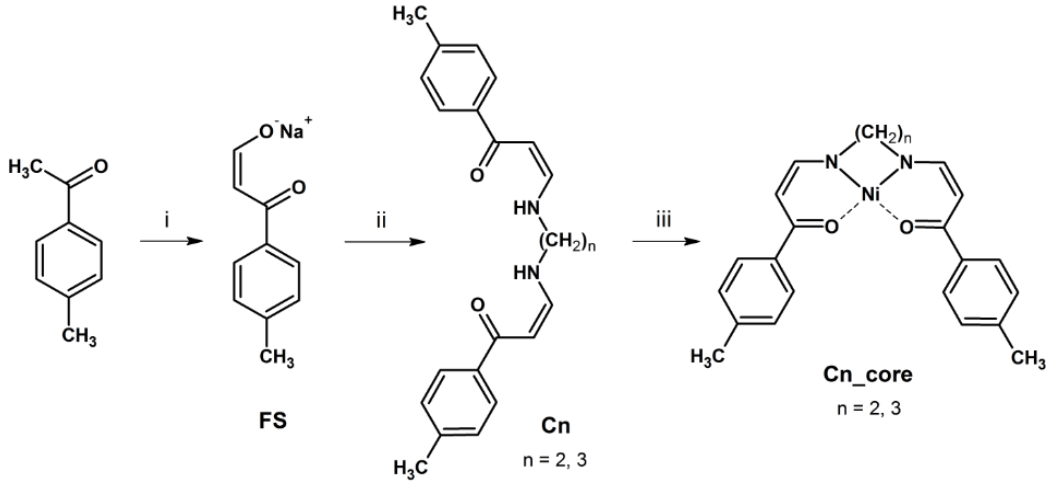

Scheme 1. General procedure for the synthesis of **C2_core** and **C3_core** compounds. Reagents and conditions: (i) Na, xylene (mixture of isomers), 140 °C, then HCOOEt, Et_2O, room temperature; (ii) $H_2N(CH_2)_nNH_2$, CH_3COOH, MeOH, 60 °C; (iii) $(CH_3COO)_2Ni$, EtOH, 70 °C.

The obtained complexes have been crystallized from the dichloromethane and methanol mixture (2:1). **C2_core** crystallizes in the triclinic *P*-1 space group with two molecules (**A** and **B**) in the independent part of unit cell. In turn, **C3_core** crystallizes in the orthorhombic *P*nma space group. The independent part of the unit cell is composed of half-molecule. The molecule lies in a special position, on a mirror plane passing through the central Ni atom and C11 atom in the propylenediamine bridge. Selected bond distances, angles and crystallographic data of both structures are given in Table 1 and Table S1 (SI), respectively. Crystal structures of **C2_core** and **C3_core** are presented in Figure 2 and Figure S5 in SI.

Both studied compounds adopt almost perfect square planar geometry, which can be quantitatively characterized by τ_4 parameter[45] proposed for tetracoordinate complexes (Table 1 and Eq. S1 in SI). The value of this parameter can range from 0 to 1 when passing from a perfect square planar to a perfect tetrahedral geometry. For the studied structures, the values are close to zero that well compliments the visual inspection of the structures. Further comparison of the structures shows that **C3_core** molecule is more bent than both **C2_core** molecules. Dihedral angles between average ONNO plane and corresponding two parts of the acacen ligand (φ_1, φ_2) are more than twice larger for **C3_core** than for both **C2_core** molecules (Table 1). A detailed description of the τ_4, φ_1 and φ_2 parameters is given in SI.

Table 1. Selected bond distances [Å] and angles [°] with their s.u. values, and structure parameters [°] of **C2_core** and **C3_core** crystal structures. Atom numbers are given in Figure 1.

	C2_core molecule A	**C2_core molecule B**	**C3_core**
Ni-O1	1.842(3)	1.844(3)	1.871(2)
Ni-O2	1.848(3)	1.852(3)	-
Ni-N1	1.847(3)	1.845(4)	1.893(2)
Ni-N2	1.838(3)	1.833(4)	-
O1-Ni-N1	94.48(13)	94.67(14)	92.22(7)
O2-Ni-N2	94.65(14)	94.44(15)	-
O1-Ni-O2	84.46(11)	84.75(12)	80.18(10)*
N1-Ni-N2	86.45(15)	86.21(17)	95.30(12)*
τ_4	0.031	0.036	0.011
φ_1	2.00	2.20	22.82
φ_2	7.46	8.54	22.82

* For **C3_core,** the angles are O1-Ni-O1′ and N1-Ni-N1′, respectively.

In the crystal structure of **C2_core**, **A** and **B** molecules create separate layers stabilized by C-H···O, C-H···C and π-π interactions, which form a herringbone packing motif (Figure 2c). Between molecules **A** and **B** there are only C-H···π interactions at the distance of 2.77 Å (C···C distance is 3.57 Å). In the **C3_core** crystal, molecules form a brick layer stacking motif (Figure 2d). In a single layer, there are no strong interactions between adjacent Ni(II) complexes. The molecules in the neighboring layers are connected by π-π, C-H···O and C-H···π interactions in the range of 2.68 Å – 2.86 Å.

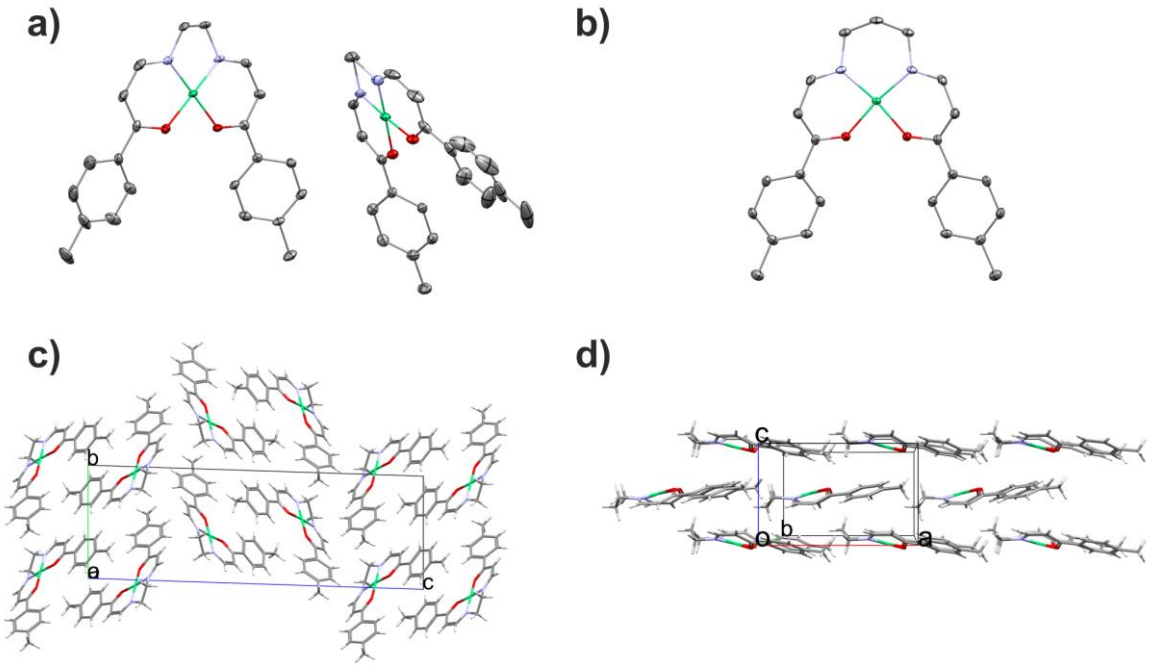

Figure 2. Crystal structures of **C2_core** (a) and **C3_core** (b); displacement parameters drawn at 50% probability level (hydrogen atoms are omitted for clarity). Crystal packing of **C2_core** - herringbone packing motif (c) and **C3_core** - brick layer stacking motif (d).

Figure S11 in SI shows the 3D Hirshfeld surfaces and 2D fingerprint plots for **C2_core** and **C3_core**. The quantitative decomposition of all intermolecular interactions shows that the C-H···H, C-H···C and C-H···O interactions are responsible for the crystal packing and formation of the three-dimensional network structure of **C2_core** and **C3_core.**

Octahedral Ni(II) complexes

Taking into account that this type of square planar Ni(II) complexes can exhibit the phenomenon of coordination-induced spin-state switching, we studied their behavior in reaction with *N*-heterocyclic aromatic amines. Pyridine as a reference, and its different derivatives, such as 3-methylpyridine, 4-methylpyridine, 3,4-dimethylpyridine, 3,5-dimethylpyridine, 3-methoxypyridine, 4-methoxypyridine (MOPy), and 4-dimethylaminopyridine (DMAP), were tested as potential axial ligands. In the case of methoxypyridine ligands, it is known that the oxygen atom of the methoxy group does not act as O-donor atom, and thus the methoxypyridine only behaves via coordination by pyridine N-donor atom. One of the first observations is that **C2_core** is particularly stable and disfavors the coordination of any axial ligands. In contrast, its structural analog with three carbon atoms in the bridge (**C3_core**) is less stable (as can be seen from comparison of Ni-O and Ni-N distances for **C2_core** and **C3_core** in Table 1) and creates octahedral complexes in reaction with pyridine (Py) and its derivatives. For 3-methylpyridine, 4-methylpyridine, 3,4-dimethylpyridine, 3,5-dimethylpyridine, and 3-methoxypyridine ligands, the reaction with **C3_core** was successful, which was observed by a color change. Despite many crystallization attempts, it was difficult to obtain a crystalline sample because the final complexes exist in the form of oil. However, in the case of Py and two other ligands, MOPy and DMAP, the crystals of the octahedral Ni(II) complexes were obtained and characterized (named accordingly: **C3_Py**, **C3_MOPy** and **C3_DMAP**). The procedure for preparation of octahedral complexes and growing their crystals can be found in the SI.

Green crystals of **C3_core** dissolve easily in pyridine forming an orange complex. Crystal structure obtained after reaction with pyridine confirm that the octahedral complex (**C3_Py**) was formed by **C3_core**, whereas square planar Ni(II) **C2_core** structure remained unchanged. **C3_Py** complex with two axially coordinated pyridine ligands crystallizes in the triclinic *P*-1 space group with one molecule in the independent part of the unit cell (Fig. S8 in SI). The bond lengths between the axial nitrogen atoms and nickel are 2.124(3) Å (top) and 2.143(3) Å (bottom), while equatorial Ni-N and Ni-O bond lengths in the acacpn part of the octahedral complex are about 0.2 Å longer compared to the initial **C3_core**, thus indicating a spin-state change upon coordination. The longer bond lengths between metal and ligand are due to a triplet electronic configuration, in which two antibonding orbitals are singly occupied, in contrast with singlet square-planar **C3_core** with shorter Ni-N/O bond lengths. Moreover, the angle between O1-Ni-O2 atoms is about 7° larger, while the other angles in this part are smaller than in

C3_core. In **C3_Py** system, the core part is an umbrella conformation similar to **C3_core** (Figure 3). However, despite the similarities in the bend of the acacpn part (φ_1 and φ_2 angles**)** in square planar **C3_core** and octahedral **C3_Py** complexes, there is a significant difference between the relative positions of phenyl substituents (larger tilt angles in **C3_Py**). The bent structure of **C3_Py** is caused by mutual orientation of axially coordinated Py ligands, which are almost perpendicular in the complex; the twist angle between the planes passing through top and bottom pyridine rings is 88.4°. The preference of perpendicular conformation for axial pyridine ligands has been observed earlier for Ni(II) complexes.[12] Selected bond distances and other parameters for the studied octahedral complexes are reported in Table 2.

Table 2. Selected bond distances [Å], angles [°], and structure parameters [°] in **C3_Py, C3_MOPy**, and **C3_DMAP** crystal structures. Atom numbers are given in Figure 1.

	C3_Py	**C3_MOPy**	**C3_DMAP mol A**	**C3_DMAP mol B**	**C3_DMAP mol C**
Ni-O1	2.049(2)	2.031(2)	2.016(2)	2.025(2)	2.034(2)
Ni-O2	2.031(2)	2.021(2)	2.042(2)	2.036(2)	2.062(2)
Ni-N1	2.055(2)	2.056(3)	2.063(3)	2.035(3)	2.062(3)
Ni-N2	2.054(3)	2.045(2)	2.066(3)	2.045(3)	2.060(3)
O1-Ni-N1	88.73(9)	89.48(9)	88.36(12)	90.60(13)	89.83(11)
O2-Ni-N2	90.54(9)	89.26(9)	88.52(13)	89.68(10)	89.56(11)
O1-Ni-O2	87.03(9)	83.90(8)	84.44(9)	83.51(9)	85.95(9)
N1-Ni-N2	93.70(10)	97.44(10)	98.68(15)	96.27(14)	94.66(13)
Ni-N3(top)	2.124(3)	2.193(3)	2.167(3)	2.150(3)	2.124(3)
Ni-N4(bottom)	2.143(3)	2.197(3)	2.154(3)	2.184(3)	2.117(3)
φ_1	25.60	8.95	0.59	11.54	11.52
φ_2	17.03	12.27	0.14	19.90	14.36

In the crystal of **C3_Py**, the molecules are stabilized mainly by C-H···H and C-H···π interactions. The top pyridine ligand interacts with the acacpn part (2.83 Å), phenyl ring (2.33 Å) and one of methylene groups from the propylenediamine bridge of neighboring molecule (2.81 Å), while the bottom pyridine molecule interacts with phenyl rings of neighboring molecules (2.38 Å – 2.87 Å) and another bottom pyridine from the opposite molecule (3.34 Å). The Hirshfeld surface analysis of **C3_Py** can be found in Figure S12, SI.

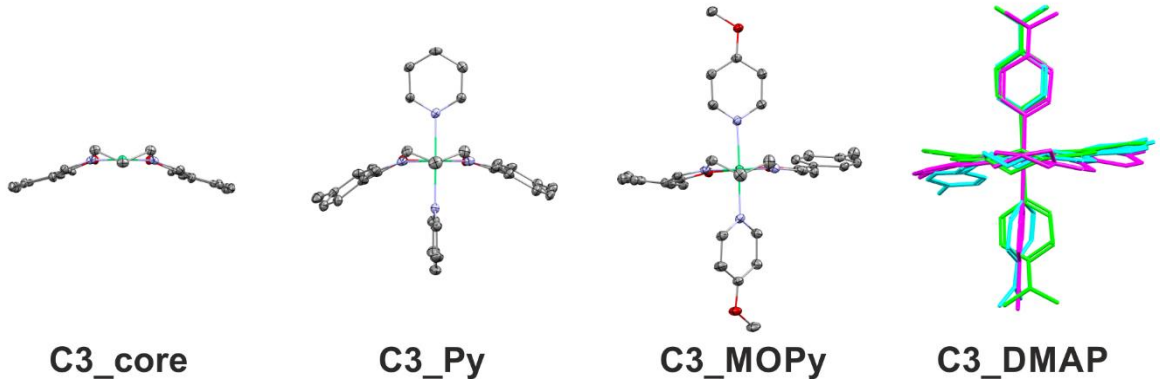

Figure 3. Crystal structures of square planar **C3_core** and its octahedral complexes with pyridine (**C3_Py**), 4-methoxypyridine (**C3_MOPy**) and 4-dimethylaminopyridine (**C3_DMAP**); displacement parameters drawn at 50% probability level. **C3_DMAP** is presented as an overlay of three molecules from the independent part of the unit cell – molecule A – green, molecule B – blue and molecule C – purple (hydrogen atoms are omitted for clarity).

The **C3_MOPy** and **C3_DMAP** complexes crystallize in the monoclinic $P2_1/c$ space group. In **C3_MOPy**, the independent part of the unit cell consists of one molecule, while in **C3_DMAP** it contains three molecules (**A**, **B**, and **C**), see Figure 3 and Figures S9, S10 in SI. The preparation of **C3_DMAP** crystals of sufficient quality for the single crystal X-ray diffraction measurements required use of a mixture of solvents (hexane:CH_2Cl_2), which were also observed in the crystal structure.

In octahedral **C3_MOPy** Ni(II) system, geometry of the acacpn part is more planar than in **C3_Py** complex, and mutual orientation of the axial ligands is also significantly different, which is clearly seen in Figure 3. In **C3_MOPy**, the axial ligands are in trans configuration and torsionally twisted with respect to each other by 29.2°. Similar orientation of axial MOPy ligands were previously observed in other crystal structures of octahedral complexes of transition metals.[46,47] The bond lengths between the axial nitrogen atoms and nickel are nearly identical (2.193(3) Å and 2.197(3) Å) and slightly longer than in **C3_Py** (2.124(3) Å and 2.143(3) Å), which is typical for high-spin complexes. The Ni-O and Ni-N bond lengths in the ONNO part of both complexes are almost similar, the difference of about 3° appears in the N-Ni-N and O-Ni-O angles (see Table 2). As in the other investigated structures, there are no strong hydrogen bonds in the **C3_MOPy** crystal. Two 4-methoxypyridine ligands interact with the phenyl ring and the axial ligand from the neighboring molecule, while the bottom ligand additionally interacts with one of methylene groups from the propylenediamine bridge. The Hirshfeld surface analysis is shown in Fig. S12.

The **C3_DMAP** crystal structure has disordered parts, especially in the propylenediamine bridge (Fig. S9 in SI). The distances between the nickel atom and equatorial donor atoms are quite similar to those found in the **C3_Py** and **C3_MOPy** crystals (Table 2). Axial ligands in the molecules **B** and **C** have perpendicular orientation relative to each other and core is bent, in contrast to the molecule **A,** with axial ligands oriented almost coplanar, characterized by planar core geometry (φ_1=0.59 and φ_2=0.14). The

twist angles for the axial ligands are 19.8°, 82.0°, and 75.8° for **A**, **B**, and **C** molecules, respectively, indicating conformational flexibility of the molecule. The different orientation of axial ligands is most likely caused by intermolecular interactions in crystal packing. Similar to the previously mentioned complexes, the structure of **C3_DMAP** crystal is mainly stabilized by C-H···H and C-H···π interactions.

Spectroscopic and thermogravimetric studies

Square planar Ni(II) complexes (**C2_core** and **C3_core**) were studied by ^{1}H NMR spectroscopy. Additionally, the experiment with deuterated pyridine was performed for both complexes. No differences between ^{1}H NMR spectrum of **C2_core** and spectrum recorded after Py-d_5 addition have been observed (see Fig. S13 in SI). Despite the pyridine addition, the complex is still unsubstituted, diamagnetic (S = 0), and has square planar geometry. In contrast, there are significant differences in spectra of **C3_core** upon addition of Py-d_5 – shifts and broadening of the signals (Figure 4). The most noticeable changes were observed for olefinic (H8, H9, H8′ and H9′) and aliphatic (H10A, H10B and H10′A, H10′B) protons - their signals changed position and shape. UV-Vis spectra also confirm that addition of pyridine to **C3_core** changes the geometry of the complex from square planar to octahedral - the maximum of absorption is shifted from 416 nm to 360 nm, respectively (Figure 5). In case of **C2_core**, no changes in UV-Vis spectrum were observed.

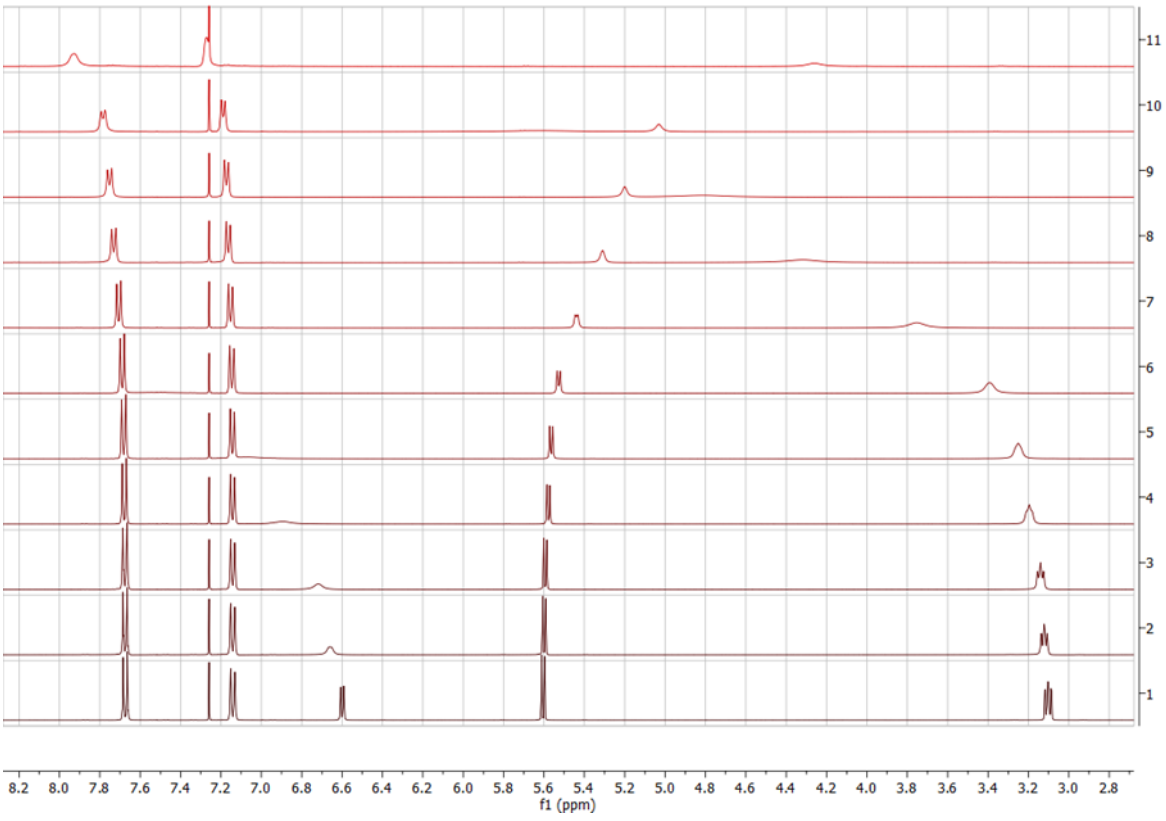

Figure 4. (1) ^{1}H NMR spectrum containing 0.03 mmol of square planar **C3_core** complex (without Py-d_5) and ^{1}H NMR spectra of **C3_core** recorded after addition of: (2) 0.003 mmol Py-d_5, (3) 0.006 mmol Py,(4) 0.012 mmol Py-d_5, (5) 0.018 mmol Py-d_5, (6) 0.030 mmol Py-d_5 (7) 0.054 mmol Py-d_5, (8) 0.090 mmol Py-d_5, (9) 0.135 mmol Py-d_5, (10) 0.21 mmol Py-d_5 and (11) 2 mmol Py-d_5, respectively.

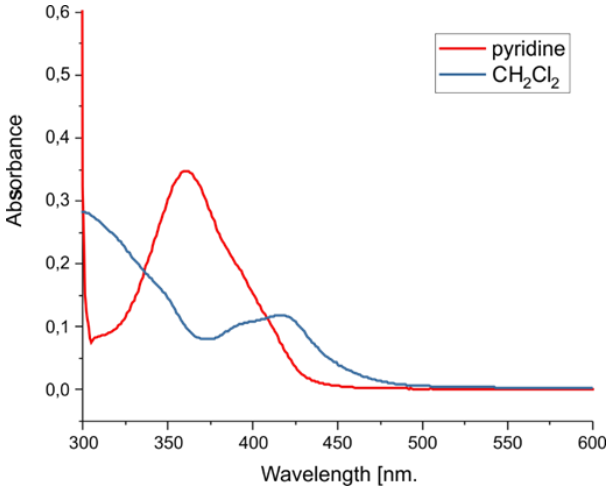

Figure 5. UV-Vis spectra of **C3_core** in CH_2Cl_2 (blue line) and **C3_core** in pyridine (red line).

The TGA curve of **C3_Py** (octahedral complex with pyridine ligands**)** shows the four-step thermal degradation process (Figure S14 in SI). The first and second mass loss takes place between 70-110 °C and 115-140 °C, releasing about 30% of the total sample mass. Most likely, it corresponds to pyridine ligands released from **C3_Py** complex. The next mass loss occurs between 290-390 °C with a loss of about 50% of the sample mass. At this point, the main Ni(II) tetradentate ONNO core begins to melt and decompose.

DFT calculations

DFT calculations of the investigated square planar Ni(II) systems were performed using their crystal structures as the initial geometries. Since Ni(II) complexes may exist in two different spin states, the geometries were optimized in singlet and triplet spin states at the BP86-D3/TDZP level, including ZORA scalar relativistic corrections and COSMO (pyridine, ε=12.4) solvation model. For a proper description of the spin-state energetics, single point calculations at the S12g/TZ2P level were additionally performed. As anticipated, the ground state of **C2_core** and **C3_core** is a singlet state (S = 0), as for other square planar complexes of Ni(II).[12,13,48,49] DFT calculations revealed large singlet-triplet (S-T) energy gaps for both complexes. ΔE(S-T) for **C2_core** is 20.9 kcal/mol, whereas for **C3_core** this gap is 15.2 kcal/mol at the S12g/TZ2P level of theory. Additionally, we compared the calculated geometries with the crystal structures. The most suitable indicator of geometrical similarity is the root-mean-square deviation (RMSD) of atomic positions in the optimized structure from their

positions in the crystal. Figure 6 shows the RMSD values calculated for both complexes studied in singlet and triplet states. Obviously, the deviations are large for the triplet, while the structures in the singlet state are very similar to those found in the crystals.

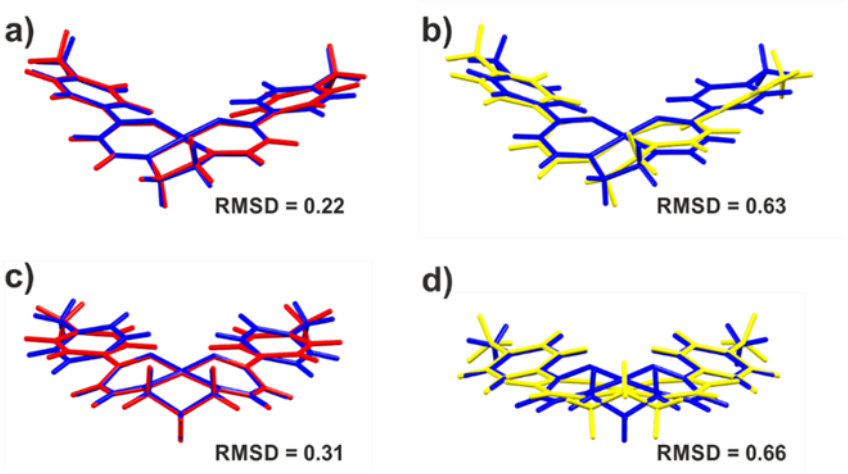

Figure 6. Overlays of the solid state structures (blue) with calculated geometries: a) **C2_core** in singlet spin state (red), b) **C2_core** in triplet spin state (yellow), c) **C3_core** in singlet spin state (red), d) **C3_core** in triplet spin state (yellow).

As mentioned before, **C2_core** does not react with pyridine to form an octahedral complex. To understand its behavior, DFT calculations were performed for the initial cores (**C2_core** and **C3_core)** with two pyridine ligands. The geometries of the complexes were optimized taking into account both spin states, although initial geometries for singlet and triplet states were identical. The calculation results show that, in the singlet state, **C2_Py** and **C3_Py** Ni(II) complexes have a sandwich-type geometry (Figure 7). The pyridine ligands are not directly bound to the nickel atom but both are located parallel to the Ni(II) core, providing π-π interactions between *N*-heterocyclic aromatic amine and tetradentate ONNO part of the core system. Alternatively, the complexes in the triplet state have an octahedral geometry with direct interactions of the pyridine ligands with the nickel atom. Thus, spin state switching occurs when going from the square planar to octahedral complex. In the case of **C3_Py**, the optimized geometry is quite similar to that in the crystal structure – the axial ligands are perpendicular to each other (twist angle is 89.0° calc. vs. 88.4° exp.) and the main core is symmetrically bent. The overlay of the crystal and optimized structures is shown in Figure 7. In turn, optimization of **C2_Py** complex leads to the structure with asymmetrically bent core as a result of π-π interactions between the bottom pyridine ligand and one of the phenyl rings of the core (3.62 Å).

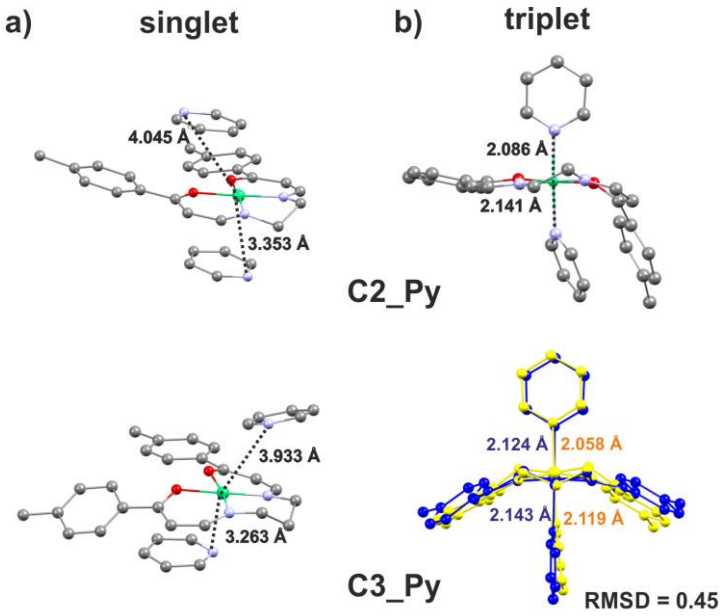

Figure 7. Structure comparison of calculated geometries for **C2_Py** and **C3_Py** in singlet (a) and triplet (b) spin states (hydrogen atoms are omitted for clarity). Last picture represents an overlay of the calculated **C3_Py** structure in triplet state (yellow, orange numbers) with its crystal structure (blue). Numbers represent the distances between nickel and N atom of pyridine.

To find a difference between octahedral **C3_Py** and **C2_Py** complexes, the bonding energy, ΔE_{bond}, of two pyridine ligands to the Ni(II) core was calculated (Table 3) at BP86-D3/TZ2P level using a Morokuma-type energy decomposition method.[50] The overall bonding energy is made up of two major components: deformation energy (ΔE_{def}) and interaction energy (ΔE_{int}). ΔE_{def} is the amount of energy required to deform the separate fragments from their equilibrium structures to their geometries in the final complex. ΔE_{int} corresponds to the actual energy change when the prepared fragments are combined to form the total system. The results show that the deformation energy of ligands is very small, ΔE_{def} (lig) < 1 kcal/mol, and the interactions between them are repulsive in both complexes, ΔE_{int} (lig-lig) is positive. The deformation energy of the core in **C2_Py** complex is significantly higher than in **C3_Py** due to its large distortion in the complex from the equilibrium geometry. In turn, the interaction energy between core and two axial ligands is greater in **C3_Py** complex. This is in agreement with Ni-N bond lengths, which are shorter in **C3_Py** than in **C2_Py** complex. As a result, this leads to a significant difference in the total bonding energy, -5.5 kcal/mol for **C2_Py** and -17.5 kcal/mol for **C3_Py**. This clearly demonstrates that the binding of pyridine ligands to the Ni(II) core is substantially more preferable in the case of **C3_core**. It can be assumed that interactions with neighboring **C2_core** molecules in the crystal are stronger than the weak coordination of axial pyridine ligands and, therefore, only square planar **C2_core** Ni(II) system crystallizes from pyridine solution, in contrast to the complex with C3 bridge.

Table 3. Interaction energies (in kcal/mol) between core and ligands, ΔE_{int} (core-lig), and between two ligands, ΔE_{int} (lig-lig), deformation energies (in kcal/mol) of core, ΔE_{def} (core), and ligands, ΔE_{def} (lig), and total bonding energies (in kcal/mol), ΔE_{bond}, for **C2_Py** and **C3_Py** complexes in triplet spin state.

	ΔE_{int}(core-lig)	**ΔE_{int}(lig-lig)**	**ΔE_{def}(core)**	**ΔE_{def}(lig)**	**ΔE_{bond}***
C2_Py	-33.9	3.5	24.3	0.6	-5.5
C3_Py	-39.2	4.1	17.0	0.6	-17.5

* $\Delta E_{bond} = \Delta E_{int}$(core-lig) + ΔE_{int}(lig-lig) + ΔE_{def}(core) + ΔE_{def}(lig)

To estimate the effect of the electron-donating groups (-OCH_3 and -NMe_2) in *para*-position of pyridine on the binding of axial ligands, the interaction energies in **C3_MOPy** and **C3_DMAP** Ni(II) complexes were also calculated. The values of ΔE_{int} are larger for **C3_MOPy** (-43.7 kcal/mol) and **C3_DMAP** (-44.3 kcal/mol) than for **C3_Py** (-39.2 kcal/mol). This trend is in line with the effect of substituents on the energy of σ-donating and π-accepting orbitals of pyridine, which participate in bonding interactions with transition metal (Fig. S15, SI). The methoxy and dimethylamino substituents increase the energy of the pyridine orbitals, thus providing better interactions with the nickel orbitals. All this confirms that the electron-donating substituents in pyridine facilitate the coordination of axial ligands to **C3_core.**

In addition, modelling of octahedral complexes with different mutual orientation of axial ligands found in crystals was carried out. When the ligands are perpendicular to each other, the acacpn Ni(II) core is strongly bent, whereas the coplanar arrangement of the ligands causes the geometry of the Ni(II) core to flatten due to steric effect (see Fig. S16 in SI). In similar crystal structures of ONNO Ni(II) complexes, the twist angle for the axial N-heterocyclic ligands in most cases exceeds 60°.[12,51,52] This is quite opposite to ONON Ni(II) type complexes, where the ligands are mostly in coplanar position to each other, and the Ni(II) core is more flattened.[53-55] As expected, the studied systems with mutual perpendicular orientation of the ligands are more stable than their conformers with the coplanar one (see Table S3 in SI). The bent Ni(II) core in the former case provides larger dispersion interactions between phenyl rings of the acacpn ligand and one of the axial N-heterocyclic ligands, which are responsible for the greater stability of such systems. However, according to the results of calculation, the conformers with the coplanar ligand arrangement are only slightly less preferable, $\Delta E_{rel} < 2$ kcal/mol, and therefore were also found in the crystal structures of **C3_MOPy** and **C3_DMAP**. An interesting case is the crystal of **C3_DMAP**, where three molecules with slightly different conformations were observed due to molecular flexibility. The global minimum is the structure with perpendicular orientation of the axial ligands resembling the molecule **B** in the crystal. Two other structures obtained during the geometry optimization of the molecules **A** and **C** are the local minima, which are 1.28 and 1.42 kcal/mol higher in energy than the global minimum. Thus, the appearance of one or another conformer in the crystal structure is determined not only by their relative stability but also by intermolecular interactions in the solid state, which ultimately can stabilize the higher-energy conformer.

CONCLUSIONS

Two square planar ONNO Ni(II) complexes with two and three carbon atoms in the diamine bridge of the ligand (**C2_core** and **C3_core)** were prepared and characterized through single crystal X-ray diffraction. Using DFT calculations, it was confirmed that in the ground state both tetradentate Ni(II) complexes are low-spin (S = 0) with large singlet-triplet energy gaps.

Unexpectedly, the length of the diamine bridge in the equatorial ligand plays a crucial role in the reaction of Ni(II) complexes with N-heterocyclic aromatic amines. Only **C3_core** can attach substituted pyridines switching from square planar low-spin to octahedral high-spin structure. This was first indicated by a color change and then confirmed by X-ray diffraction. DFT calculations revealed that **C2_core** does not form an octahedral complex with pyridine due to high deformation energy of the core required for its formation.

The electron-donating substituents on the pyridine ring facilitate the coordination of axial ligands to **C3_core**. Moreover, complexes with mutual perpendicular orientation of the axial ligands are more stable than their conformers with coplanar orientation because of larger dispersion interactions between core and one of the axial N-heterocyclic ligands.

Our findings show that not only nature of the equatorial ligand but also its small geometric changes are important in the design of new transition metal-based complexes with coordination-induced spin-state switching behavior.

ACKNOWLEDGEMENTS

The work has been performed under the Project HPC-EUROPA3 (INFRAIA-2016-1-730897), with the support of the EC Research Innovation Action under the H2020 Programme; in particular, K.P. gratefully acknowledges the support of the Institute of Computational Chemistry and Catalysis, University of Girona and the computer resources and technical support provided by Barcelona Supercomputing Center (BSC). The authors thank Dr. Wanda Sicińska (University of Warsaw) for useful discussions. The authors thank A. Gajda and Prof. G. Litwinienko (University of Warsaw) for the opportunity to carry out thermogravimetric analysis on the TA Instruments Q50 Thermal Gravimetric Analyzer. M.S. and O.A.S. acknowledge financial support from the Spanish MINECO (projects CTQ2017‐85341‐P, PID2020-113711GB-I00, and FJCI‐2017‐32757 to O.A.S.) and the Catalan DIUE (2017SGR39).

Keywords

Transition metals, Nickel, Octahedral complex, Reactivity, Crystal structure, Density functional calculations

Conflict of Interest

The authors declare no conflict of interest.

Supporting Information

Experimental details, additional figures and tables, and Cartesian coordinates.

REFERENCES

[1] S. Thies, C. Bornholdt, F. Köhler, F. D. Sönnichsen, C. Näther, F. Tuczek, R. Herges, *Chem. Eur. J.* **2010**, *16*, 10074-10083.

[2] M. Dommaschk, F. Gutzeit, S. Boretius, R. Haag, R. Herges, *Chem. Commun*. **2014**, *50*, 12476-12478.

[3] M. Dommaschk, V. Thoms, C. Schütt, C. Näther, R. Puttreddy, K. Rissanen, R. Herges, *Inorg. Chem.* **2015**, *54*, 9390-9392.

[4] J. Linares, E. Codjovi, Y. Garcia, *Sensors* **2012**, 12, 4479-4492.

[5] K. Boukheddaden, M. H. Ritti, G. Bouchez, M. Sy, M. M. Dîrtu, M. Parlier, J. Linares, Y. Garcia, *J. Phys. Chem. C* **2018**, 122, 7597-7604.

[6] A. Bousseksou, G. Molnar, L. Salmon, W. Nicolazzi, *Chem. Soc. Rev*. **2011**, *40*, 3313-3335.

[7] M. A. Halcrow, *Spin-Crossover Materials: Properties and Applications*, John Wiley & Sons Ltd, Chichester, **2013**, p. 564.

[8] B. Benaicha, K. Van Do, A. Yangui, N. Pittala, A. Lusson, M. Sy, G. Bouchez, H. Fourati, C. J. Gomez-Garcia, S. Triki, K. Boukheddaden, *Chem. Sci*. **2019**, *10*, 6791-6798.

[9] H. Kurz, K. Schötz, I. Papadopoulos, F. W. Heinemann, H. Maid, D. M. Guldi, A. Köhler, G. Hörner, B. A. Weber, *J. Am. Chem. Soc.* **2021**, *143*, 3466-3380.

[10] E.-G. Jäger, K. Schuhmann, H. Görls, *Inorg. Chim. Acta* **1997**, *255*, 295-305.

[11] Q. Meng, J. K. Clegg, K. A. Jolliffe, L. F. Lindoy, M. Lan, G. Wei, *Inorg. Chem. Comm.* **2010**, *13*, 558-562.

[12] M. Klaß, J. Krahmer, C. Näther, F. Tuczek, *Dalton. Trans*. **2018**, *47*, 1261-1275.

[13] H. Brandenburg, J. Krahmer, K. Fischer, B. Schwager, B. Flöser, C. Näther, F. Tuczek, *Eur. J. Inorg. Chem*. **2018**, *5*, 576-585.

[14] S. Shaw, J. D. White, *Chem. Rev*. **2019**, *119*, 9381–9426.

[15] U. Tomažin, U. Grošelj, M. Počkaj, F. Požgan, B. Štefane, J. Svete, *ACS Comb. Sci.* **2017**, *19*, 386–396.

[16] Ch. Lochenie, K. G. Wagner, M. Karg, B. Weber, *J. Mater. Chem. C* **2015**, *3*, 7925-7935.

[17] M. C. Heffern, V. Reichova, J. L. Coomes, A. S. Harney, E. A. Bajema, T. J. Meade, *Inorg. Chem.* **2015**, *54*, 9066-9074.

[18] L. M. Matosziuk, R. J. Holbrook, L. M. Manus, M. C. Heffern, M. A. Ratner, T. J. Meade, *Dalton Trans.* **2013**, *42*, 4002-4012.

[19] B. Weber, W. Bauer, J. Obel, *Angew. Chem. Int. Ed.* **2008**, *47*, 10098-10101.

[20] B. Weber, E.-G. Jäger, *Eur. J. Inorg. Chem.* **2009**, 465-477.

[21] C. Hansch, A. Leo, R. W. Taft, *Chem. Rev*. **1991**, *91*, 165-195.

[22] APEX2, Bruker AXS Inc., Madison, Wisconsin, USA, 2013.

[23] SAINT, Bruker AXS Inc., Madison, Wisconsin, USA, 2013.

[24] SADABS, Bruker AXS Inc., Madison, Wisconsin, USA, 2012.

[25] TWINABS, Bruker AXS Inc., Madison, Wisconsin, USA, 2012.

[26] G. M. Sheldrick, *Acta Cryst.* **2015**, *A71*, 3-8.

[27] G. M. Sheldrick, *Acta Cryst.* **2015**, *C71*, 3-8.

[28] A. J. C. Wilson, *International Tables for Crystallography*, vol. C, Kluwer, Dordrecht, **1992**.

[29] G. M. Sheldrick, *Acta Cryst*. **2008**, *A64*, 112-122.

[30] L. J. Bourhis, O. V. Dolomanov, R. J. Gildea, J. A. K. Howard, H. Puschmann, *Acta Cryst.* **2015**, *A71*, 59-75.

[31] O. V. Dolomanov, L. J. Bourhis, R. J. Gildea, J. A. K. Howard, H. Puschmann, OLEX2: a complete structure solution, refinement and analysis program. *J. Appl. Cryst.* **2009**, *42*, 339-341.

[32] C. F. Macrae, I. Sovago, S. J. Cottrell, P. T. A. Galek, P. McCabe, E. Pidcock, M. Platings, G. P. Shields, J. S. Stevens, M. Towler, P. A. Wood, Mercury 4.0: from visualization to analysis, design and prediction. *J. Appl. Cryst.* **2020**, *53*, 226-235.

[33] M. A. Spackman, D. Jayatilaka, *CrystEngComm* **2009**, *11*, 19-32.

[34] M. J. Turner, J. J. McKinnon, S. K. Wolff, D. J. Grimwood, P. R. Spackman, D. Jayatilaka, M. A. Spackman, CrystalExplorer 17.5, The University of Western Australia, **2017**.

[35] M. A. Spackman, J. J. McKinnon, *CrystEngComm* **2002**, *4*, 378-392.

[36] G. te Velde, F. M. Bickelhaupt, E. J. Baerends, C. Fonseca Guerra, S. J. A. van Gisbergen, J. G. Snijders, T. Ziegler, *J. Comput. Chem*. **2001**, *22*, 931-967.

[37] ADF2019.3, SCM, Theoretical Chemistry, Vrije Universiteit, Amsterdam, The Netherlands, http://www.scm.com

[38] A. D. Becke, *Phys. Rev. A* **1988**, *38*, 3098-3100.

[39] J. P. Perdew, *Phys. Rev. B* **1986**, *33*, 8822-8824.

[40] E. van Lenthe, A. E. Ehlers, E. J. Baerends, *J. Chem. Phys*. **1999**, *110*, 8943-8953.

[41] S. Grimme, J. Antony, S. Ehrlich, H. Krieg, *J. Chem. Phys*. **2010**, *132*, 154104.

[42] C. C. Pye, T. Ziegler, *Theor. Chem. Acc*. **1999**, *101*, 396-408.

[43] M. Swart, *Chem. Phys. Lett*. **2013**, *580*, 166-171.

[44] S. Stepanović, L. Andjelković, M. Zlatar, K. Andjelković, M. Gruden-Pavlović, M. Swart, *Inorg. Chem.* **2013**, *52*, 13415-13423.

[45] L. Yang, D. R. Powell, R. P. Houser, *Dalton Trans*. **2007**, 955-964.

[46] M. K. Peters, C. Näther, R. Herges, *Acta Cryst*. **2019**, *E75*, 762-765.

[47] F. A. Mautner, M. Traber, R. C. Fischer, K. Reichmann, R. Vicente, *Polyhedron* **2018**, *144*, 30-35.

[48] G. Heitmann, Ch. Schütt, J. Gröbner, L. Huber, R. Herges, *Dalton Trans.* **2016**, *45*, 11407-11412.

[49] F. Gutzeit, M. Dommaschk, N. Levin, A. Buchholz, E. Schaub, W. Plass, C. Näther, R. Herges, *Inorg. Chem*. **2019**, *58*, 12542-12546.

[50] G. te Velde, F. M. Bickelhaupt, E. J. Baerends, C. Fonseca Guerra, S. J. A. van Gisbergen, J. G. Snijders, T. Ziegler, *J. Comput. Chem.* **2001**, *22*, 931-967.

[51] J. Oldengott, F. L .B. Röhs, A. Stammler, H. Bogge, T. Glaser, *Z. Anorg. Allg. Chem.* **2017**, *643*, 819-825.

[52] C.-G. F. von Richthofen, A. Stammler, H. Bogge, T. Glaser, *Eur. J. Inorg. Chem.* **2011**, 49-52.

[53] M. C. G. Souza, L. da C. Ferreira, N. M. Comerlato, G. B. Ferreira, L. do Canto Visentin, *Acta Cryst*. **2012**, *E68*, m1470.

[54] Ch.-Z. Zheng, L. Wang, J. Liu, *Acta Cryst*. **2011**, *E67*, m978.

[55] M. K. Singh, S. Roy, A. Hansda, S. Kumar, M. Kumar, V. Kumar, S. C. Peter, R. P. John, *Polyhedron* **2017**, *126*, 100-110.

Table of Contents

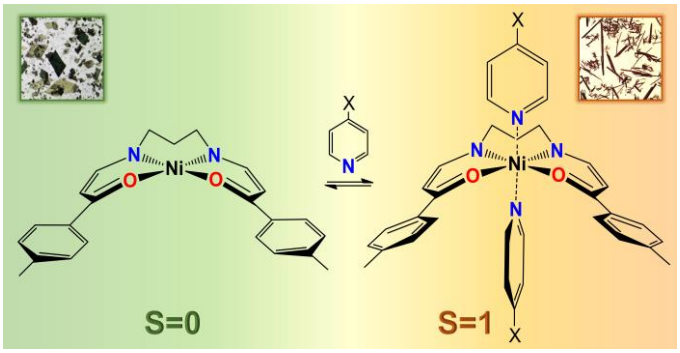

Comparison of two synthesized and characterized square planar Ni(II) complexes showed that the length of the diamine bridge in the equatorial ligand plays a crucial role in the reaction with N-heterocyclic aromatic amines. Only complex with propylenediamine bridge attaches pyridine derivatives switching from square planar low-spin to octahedral high-spin structure.